

**University of South Florida**

---

**From the Selected Works of Philip J. Motta**

---

July, 1990

# An Analytical Electron Microscopy Study of Iron-Rich Teeth from the Butterflyfish (*Chaetodon-Ornatissimus*)

N. H. C. Sparks

Philip J. Motta, *University of South Florida*

R. P. Shellis

V. J. Wade

S. Mann



Available at: [https://works.bepress.com/philip\\_motta/2/](https://works.bepress.com/philip_motta/2/)

## AN ANALYTICAL ELECTRON MICROSCOPY STUDY OF IRON-RICH TEETH FROM THE BUTTERFLYFISH (*CHAETODON ORNATISSIMUS*)

By N. H. C. SPARKS<sup>1</sup>, P. J. MOTTA<sup>2</sup>, R. P. SHELLIS<sup>3</sup>, V. J. WADE<sup>1</sup> AND  
S. MANN<sup>1</sup>

<sup>1</sup>*School of Chemistry, University of Bath, Claverton Down, Bath BA2 7AY, UK,*

<sup>2</sup>*Department of Biology, University of South Florida, Tampa, FL 33620–5150,*

*USA and* <sup>3</sup>*MRC Dental Unit, The Dental School, Lower Maudlin Street,  
Bristol BS1 2LY, UK*

*Accepted 8 February 1990*

### Summary

Iron is known to be a common constituent of vertebrate teeth, yet little is known about the form it takes or the extent to which it modifies the structural properties of the tooth. Analytical electron microscopy was used to study the iron-rich tooth cap of the butterflyfish *Chaetodon ornatissimus* Cuvier, 1831. Images of thin sections of the tooth cap showed three distinct layers of hydroxyapatite crystals; a densely packed cuticle, a crystallographically organized superficial enameloid and a randomly oriented inner enameloid. Energy dispersive X-ray analysis (edXa) showed that iron was concentrated in the cuticular layer of the tooth cap, the concentration increasing to a maximum at the tip. Elemental analysis showed the level of calcium to be inversely related to iron concentration. An identical relationship was found for synthetic iron-doped hydroxyapatite. The implications of these results for the functional role of iron in the tooth caps are discussed.

### Introduction

Iron has long been recognized as a constituent of the tooth surface of many invertebrates and vertebrates (Schmidt, 1958, 1959; Schmidt and Keil, 1971; Preuschoft *et al.* 1974; Shellis and Berkovitz, 1976; Motta, 1985), although its function, if any, is uncertain. Some authors have suggested that iron serves to harden the tooth, making it more resistant to abrasion and cracking (Preuschoft *et al.* 1974; Shellis and Berkovitz, 1976). Indeed, Motta (1987) suggested that the level of iron in the tooth cap of chaetodontid butterflyfishes was related to the hardness of the coralline prey.

The iron in the outer layer of vertebrate teeth appears to be deposited by cells of the inner dental epithelium during tooth development (Randall, 1966; Garant, 1970). Unlike the invertebrates, in which the iron has been shown to be present as the oxides magnetite, lepidocrocite or goethite (Lowenstam, 1967), the miner-

Key words: iron-rich teeth, butterflyfish, hydroxyapatite.

alogy of the iron in vertebrate teeth is not certain. Kerr (1960) believed that the iron in axolotl teeth was present as haematite ( $\alpha\text{-Fe}_2\text{O}_3$ ) and observations by Selvig and Halse (1975) indicate that in rat incisor enamel the iron is not present as a separate phase but is bound to the surface of the hydroxyapatite crystals.

The aim of this study was twofold. First, to determine the spatial localization of iron within the cap of the butterflyfish jaw tooth, using energy dispersive X-ray analysis, and to identify its structural form. Second, to examine the potential of iron-doped synthetic hydroxyapatite as a model system for these biogenic materials.

## Materials and methods

### *Fish teeth*

#### *Specimen preparation*

Jaw teeth from the butterflyfish *Chaetodon ornatissimus*, cleaned of cellular material, were obtained according to previously described methods (Motta, 1984). The teeth selected for examination were those with the darkest coloration, as iron content and coloration have been positively correlated (Motta, 1987).

#### *Scanning electron microscopy (SEM)*

Sections comprising four teeth (cap, shaft and the underlying bone) were dissected from the jaw, serially dehydrated in acetone and critical-point dried. The sections were mounted on aluminium stubs using colloidal carbon and sputter-coated with gold/palladium. The specimens were examined with a Jeol 35C electron microscope operated at 20 keV.

#### *Transmission electron microscopy (TEM)*

Tooth caps were separated from the lower jaw by cutting through the tooth shaft. The caps were dehydrated in an acetone series and embedded in Taab resin. The teeth were oriented so that longitudinal sections could be cut. Ultra-thin sections were made using a diamond knife fitted to a Reichert OMU3 ultramicrotome and placed on nitrocellulose-covered, carbon-coated copper mesh grids. The sections were examined using a Jeol 2000FX electron microscope operated at 200 keV with an objective aperture of 80  $\mu\text{m}$ . This instrument was capable of a point-to-point resolution of 0.28 nm. Electron diffraction patterns were recorded in the selected area mode.

#### *Energy dispersive X-ray analysis (edXa)*

Energy dispersive X-ray analysis was carried out in both scanning and transmission modes. The SEM was fitted with an inclined, and the TEM with a horizontal, ultra-thin-window, Li-drifted detector (Link AN10000 and associated software).

Five teeth were examined using SEM. Each tooth cap was analysed (areas

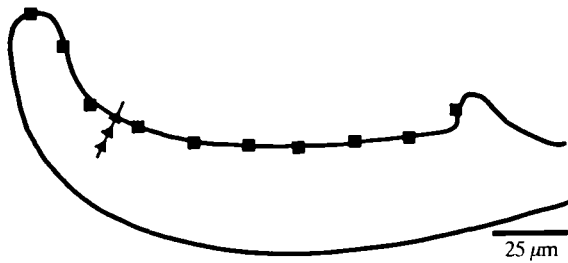


Fig. 1. Schematic diagram of a thin section of a tooth cap showing the approximate position of the sites examined by energy dispersive X-ray analysis. Lingual edge (■); normal to the tooth-cap surface (▲).

approximately  $20\ \mu\text{m}$  in diameter, for 100 s) at 30 sites. The shaft was analysed at five sites. The smaller probe diameter of the TEM enabled areas approximately  $2\ \mu\text{m}$  in diameter to be analysed (for 100 s) at approximately  $15\ \mu\text{m}$  intervals along an ultra-thin longitudinal section of the lingual edge of the cap (Fig. 1). Analyses were also carried out at intervals of approximately  $2\ \mu\text{m}$  along a line perpendicular to the tooth surface which bisected the tooth long axis at approximately one-third of the distance from the tip (Fig. 1).

Counts due to background interference were deducted (Link AN10000 software) and the  $K\alpha$  and  $K\beta$  peaks for calcium, phosphorus and iron were expressed as a percentage of the total number of counts.

#### *Synthetic hydroxyapatite*

Two samples of hydroxyapatite [ $\text{Ca}_5(\text{PO}_4)_3\text{OH}$ ], one doped with iron (iron hydroxyapatite), were synthesised at pH 7.4 and  $37^\circ\text{C}$ , by slow addition of  $\text{Ca}(\text{CH}_3\text{COO})_2$  ( $0.1\ \text{mol l}^{-1}$ ) and  $(\text{NH}_4)_3\text{PO}_4$  ( $0.06\ \text{mol l}^{-1}$ ) solutions to  $\text{CH}_3\text{COONH}_4$  ( $1.3\ \text{mol l}^{-1}$ ) solution.  $\text{FeCl}_3$  was added to one  $\text{Ca}(\text{CH}_3\text{COO})_2$  solution at the atomic ratio 1:10 (Fe:Ca) (Okazaki *et al.* 1985). The slurries were incubated for 2 h at  $37^\circ\text{C}$  followed by 2 days at  $25^\circ\text{C}$  prior to filtration, exhaustive washing and drying at  $25^\circ\text{C}$  over  $\text{P}_2\text{O}_5$ .

#### *Transmission electron microscopy – synthetic hydroxyapatites*

The hydroxyapatite samples were prepared for TEM by suspending powders in chloroform (Analar grade), briefly sonicating (3 s), and then loading on nitrocellulose-covered, carbon-coated copper grids. The grids were viewed, and electron diffraction patterns recorded from single crystals. These were indexed on the basis of a hexagonal unit cell (space group  $\text{P6}_3/\text{M}$ ) with unit cell dimensions  $a = b = 0.9418\ \text{nm}$ ,  $c = 0.6884\ \text{nm}$ .

#### *X-ray diffraction*

X-ray diffraction measurements were carried out using a Philips 4 kW generator (PW1730/10) with a long fine-focus 2 kW copper target X-ray tube (PW2273/20)

and a xenon proportional counter (PW1711/10). As a sample size of approximately 1 g was required to fill the specimen holder, only synthetic hydroxyapatite/iron-doped hydroxyapatite samples were analysed.

### *Atomic absorption*

The synthetic samples were dissolved in hydrochloric acid and then diluted to approximately 5 p.p.m. Ca to bring them within the range of the standards. The solutions were run on a Varian AA-275 atomic absorption spectrophotometer.

## **Results**

### *Butterflyfish teeth*

Butterflyfish jaw teeth lie on the premaxilla and dentary bones, forming rows of varying number. Inner teeth are usually smaller and more villiform, and outer or more labial teeth are more spatulate. The teeth are composed of a cap and a shaft (Fig. 2) which is firmly ankylosed to the bony pedestals. The cuticle, which is deposited during tooth development, is restricted to the tooth cap. Occasionally, abrasion of the pointed tooth cap results in a more rounded profile.

Perl's reaction was used to confirm the presence of iron in a sample of teeth from the butterflyfish (*C. ornatissimus*). This test uses  $2 \text{ mol l}^{-1}$  hydrochloric acid to dissolve the ferric iron which is then reacted with potassium ferrocyanide to form a blue precipitate of ferric ferrocyanide. The tooth caps, but not the shafts, were positive for iron, indicating that the iron in the cap must be in an ionizable state or relatively loosely bound since no reaction occurs if the iron is firmly bound in a complex molecule (Miles, 1963).

Elemental analysis (edXa) using a scanning electron microscope (SEM) showed calcium and phosphorus to be the main constituents of the tooth-cap surface with only low levels of iron present (data not shown). The low level of iron recorded was not consistent with Perl's reaction which showed the tooth cap to be coated with iron. The failure of the edXa system, when used under SEM conditions, to detect comparable quantities of iron may be due in part to substantial absorption of the emitted iron  $K\alpha$  X-rays by the curved surface of the cap (Fig. 2).

In thin sections, the tooth cap was composed of three crystal layers; a cuticular and a superficial enameloid layer (Fig. 3) and, towards the centre of the tooth, an inner enameloid layer. Electron diffraction powder patterns gave  $d$ -spacings for each layer corresponding to standard hydroxyapatite  $d$ -spacings (data not shown). Thus, the differences in the layers result from a change in the orientation and morphology of the constituent hydroxyapatite crystals. There was no electron diffraction evidence for the presence of crystalline iron minerals.

The cuticular layer, which covered the outer surface of the tooth cap, appeared as an electron-dense band approximately 300 nm thick (Fig. 4). The crystals were packed closely together to form a smooth, fissure-free, outer surface. Although there was no evidence of a preferred crystal orientation in the diffraction patterns, a number of the crystals imaged at high resolution were oriented such that the

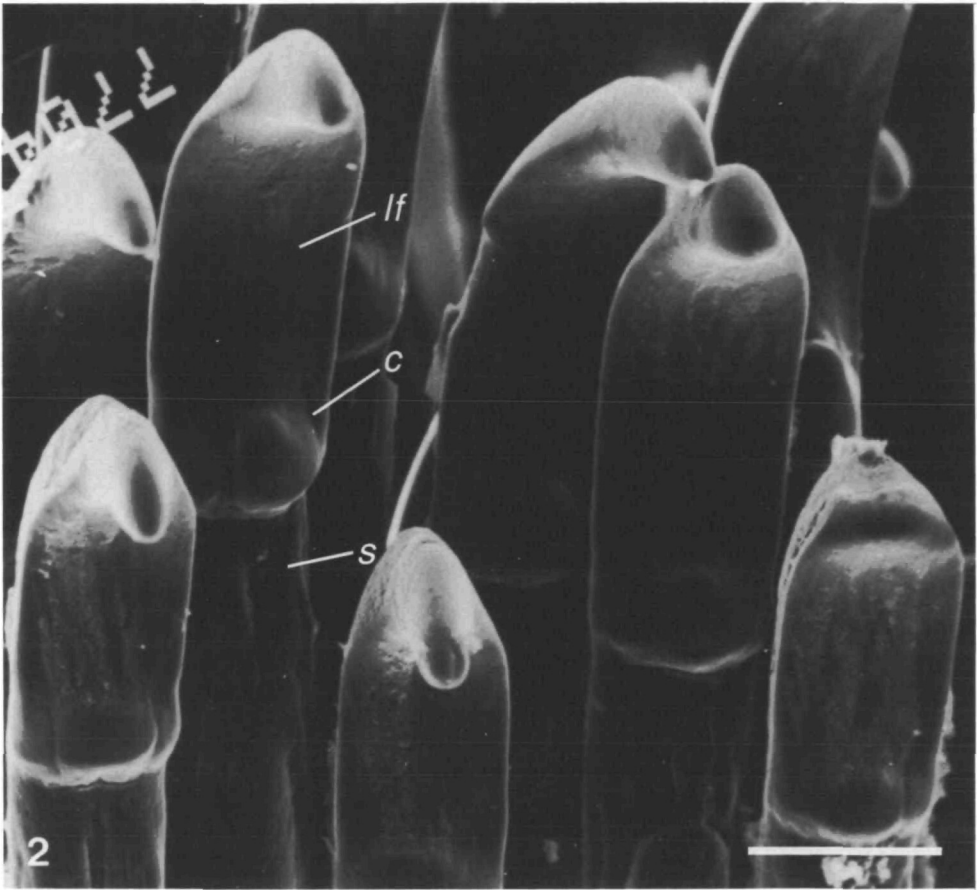


Fig. 2. Scanning electron micrograph of tooth caps (*c*) from a butterflyfish showing the connection with the shaft (*s*). Lingual face, *lf*. Scale bar, 50  $\mu\text{m}$ .

(0002) and  $(10\bar{1}0)$  lattice planes were parallel and perpendicular, respectively, to the cuticle surface (Fig. 5). This indicates that the crystal *c*-axis in these crystals was preferentially aligned perpendicular to the cuticle surface.

The superficial enameloid layer consisted of elongated crystals (approximately  $100\text{ nm} \times 12\text{ nm} \times 12\text{ nm}$ ), which were oriented in 'bundles' along the long axis of the tooth cap (Figs 6, 7). The bundles were separated by elongated crystals viewed in cross-section. This layer appears, therefore, to be formed from alternating layers of unidirectional bundles of crystals. The concept of the superficial enameloid of *C. ornatissimus* having a 'woven structure' is consistent with the findings of Schmidt and Keil (1971), Reif (1973) and Shellis and Berkovitz (1976). In contrast, the inner enameloid layer consisted of loosely packed, randomly oriented, irregular plate-like crystals, approximately 50 nm in length (Figs 8, 9). There was no evidence for dentine-type processes in the tooth cap of the butterflyfish. This was consistent with the findings of Motta (1984).

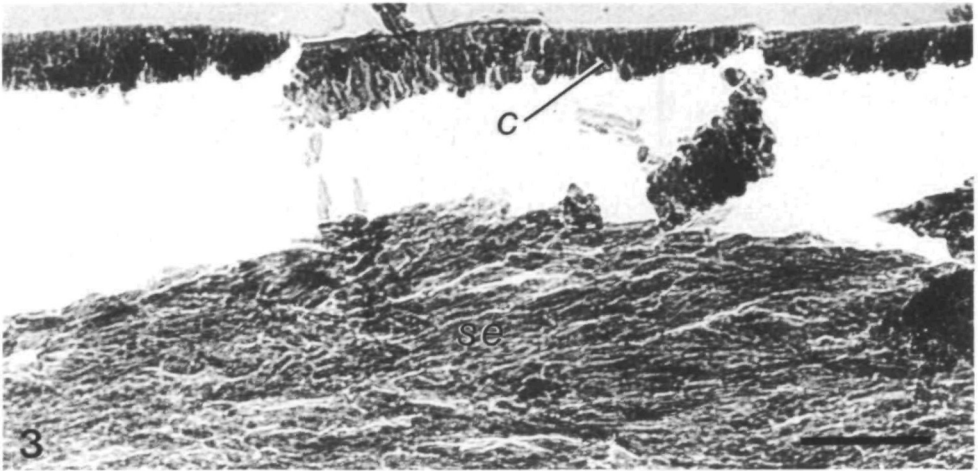


Fig. 3. Transmission electron micrograph of the cuticular layer (*c*) and underlying superficial enameloid (*se*). The gap between the two layers is an artefact of specimen preparation. Scale bar, 500 nm.



Fig. 4. Micrograph of the electron-dense cuticular layer. Note the lack of fissuring across the layer. Scale bar, 100 nm.

Elemental analysis (edXa) of the lingual edge of the cap section showed iron to be present in conjunction with calcium and phosphorus (Fig. 10). Iron counts were maximal (7.54%) at the tip of the cap, decreasing to, and then levelling out at about 3% midway between the tip and the base of the cap (Fig. 11). No iron was detected in the shaft of the tooth. Phosphorus levels were stable throughout (about 32% of the total counts), a feature noted previously by Halse (1973) in his study of iron in rat incisor. Calcium levels were inversely related to iron levels

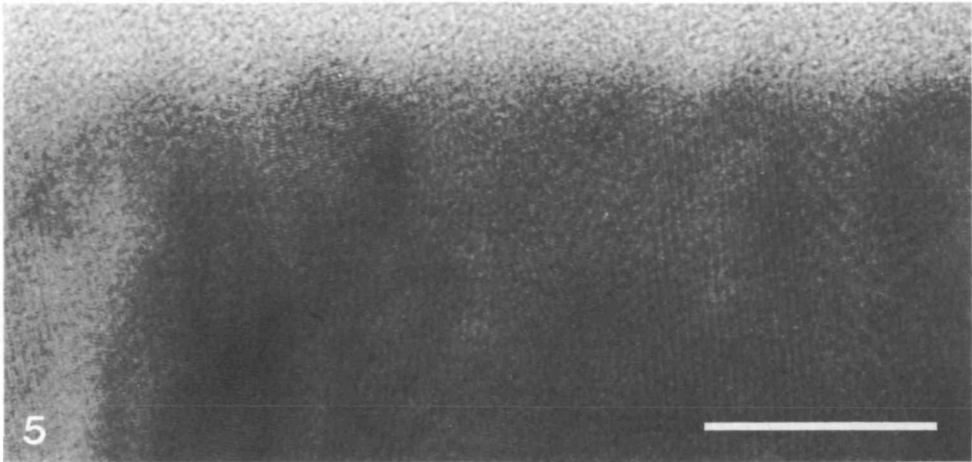


Fig. 5. High-resolution transmission micrograph of the cuticular layer showing the smooth outer surface, (0002) and (1010) lattice planes running parallel and perpendicular, respectively, to the surface. Scale bar, 20 nm.

(linear correlation coefficient of  $r = -0.97$ ,  $P < 0.001$ , Fig. 12). Iron was confined to the cuticular layer of the cap, the counts falling below detectable levels  $2 \mu\text{m}$  from the cap surface (Fig. 13).

#### *Synthetic iron-doped hydroxyapatite*

The atomic absorption spectra for a sample of synthetic iron-doped hydroxyapatite (4.2% iron w/w) showed iron to be present at an atomic ratio of 1:6.8 (Fe: Ca). The iron-doped sample showed an additional infrared peak at  $1565 \text{ cm}^{-1}$  (Fig. 14) due to N-H vibrations from occluded ammonium ions. Carbonate vibrational modes were observed in infrared spectra of both doped and non-doped samples, consistent with the preparation having been made in air.

The X-ray diffraction patterns for the non-doped and iron-doped hydroxyapatites were identical, each showing the major  $d$ -spacings for hydroxyapatite. Thus, there was no apparent change in the cell dimensions for the doped sample under these levels of iron incorporation.

The particles of synthetic hydroxyapatite were plate-like with an irregular outline (Fig. 15). There was no visible difference between the iron-doped and the non-doped samples. Lattice fringes (data not shown) were a feature of all the particles, indicating that they were single crystals with a high degree of structural perfection. Selected area electron diffraction (SAD) patterns (Fig. 16) were characteristic of single crystals and indicated that the top of the plates corresponded to the prismatic (1100) face of hydroxyapatite. There was no difference between the SAD patterns of the doped and the non-doped samples (data not shown).

Although edXa data on individual crystals indicated that there was a wide variation in the amount of iron incorporated into individual hydroxyapatite

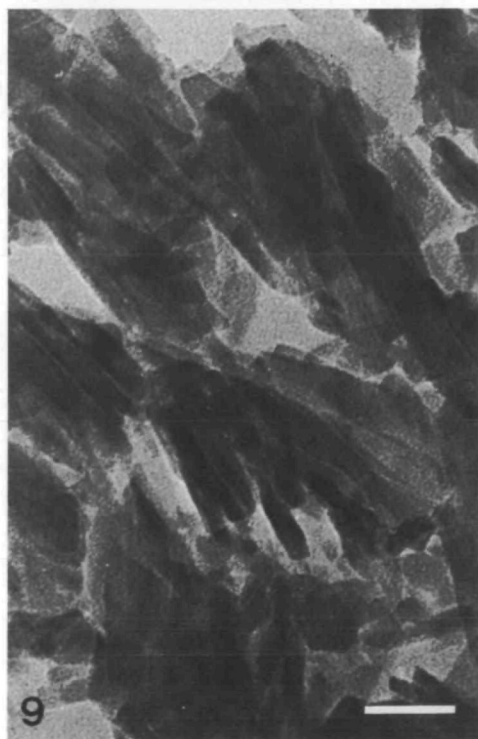
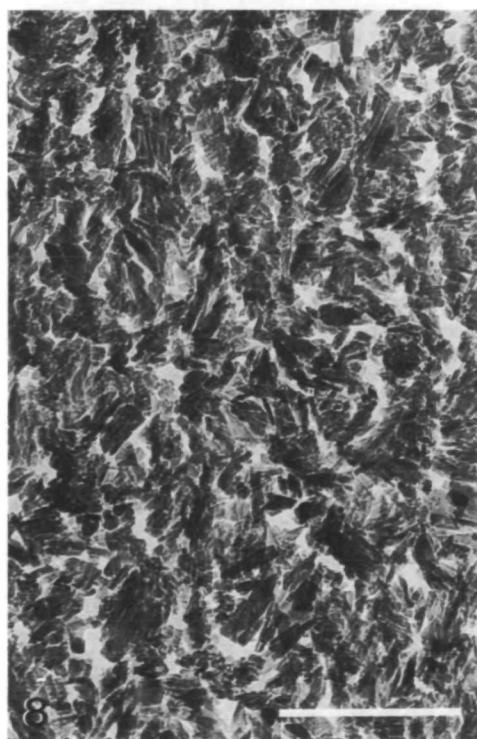
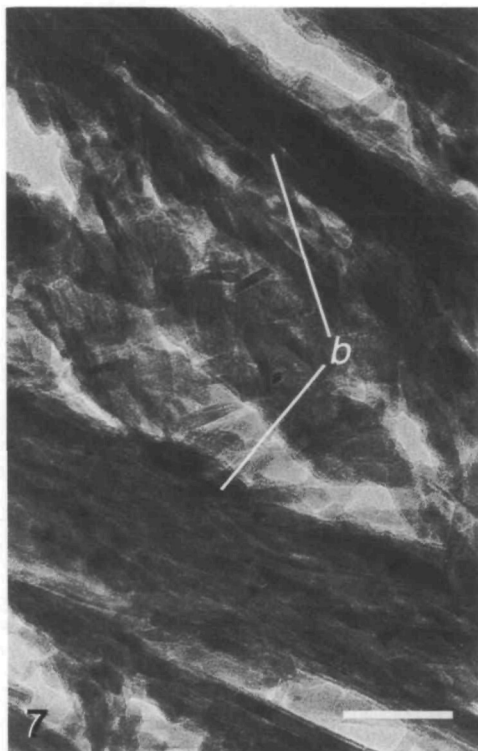


Fig. 6. Elongated hydroxyapatite crystals in the superficial enameloid layer arranged in 'bundles' (*b*) running parallel to the long axis of the tooth cap. The small crystals separating the bundles are probably elongated crystals viewed in cross-section. Scale bar, 500 nm.

Fig. 7. Detail from Fig. 6 showing the oriented bundles (*b*) of hydroxyapatite crystals. Scale bar, 100 nm.

Fig. 8. TEM of the inner enameloid layer showing loosely packed, randomly oriented hydroxyapatite crystals. Scale bar, 500 nm.

Fig. 9. Detail from Fig. 8. Scale bar, 50 nm.

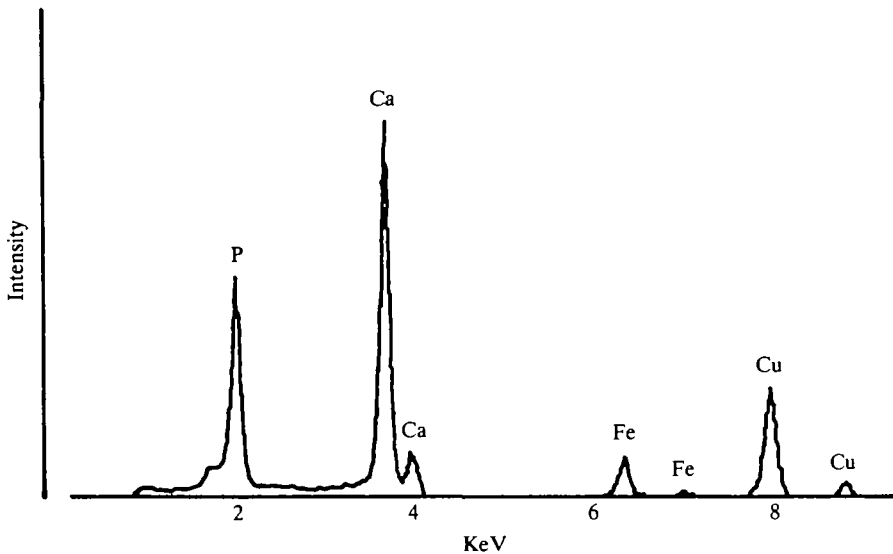


Fig. 10. Energy dispersive X-ray analysis spectrum from the cuticular layer (TEM mode).

crystals (Fig. 17), the inverse relationship ( $r = -0.99$ ,  $P < 0.001$ ) between the iron and calcium counts was consistent for all crystals examined (Fig. 18). Phosphorus levels remained stable in the crystals, being independent of changes in the iron/calcium ratio (Fig. 17). No iron was detected in the non-doped sample.

### Discussion

The tooth cap of the butterflyfish is composed of three mineralized (hydroxyapatite) layers; an iron-rich cuticle, the superficial enameloid and the inner enameloid. Each layer is formed from morphologically distinct arrangements of hydroxyapatite crystals.

The cuticular layer is a common feature of fish teeth, although its structure varies from species to species. For example, in sharks' teeth (Schmidt and Keil, 1971; Reif, 1973) it takes the form of large randomly oriented crystals, while in the

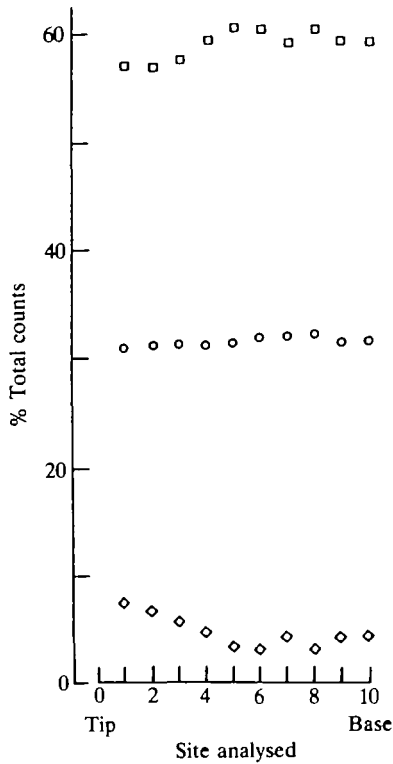


Fig. 11. Comparison of calcium ( $\square$ ), phosphorus ( $\circ$ ) and iron ( $\diamond$ ) counts (edXa) from the cuticular layer (lingual edge) of the tooth cap. The sites were approximately  $15\ \mu\text{m}$  apart.

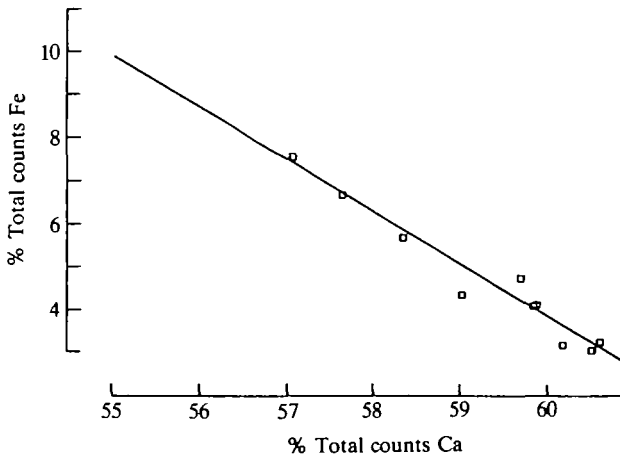


Fig. 12. Linear correlation of iron and calcium counts (edXa) from the cuticular layer (lingual edge) of the tooth cap;  $r = -0.97$ ,  $P < 0.001$ .

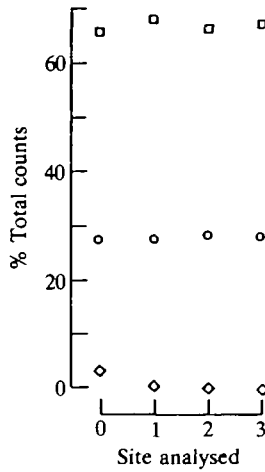


Fig. 13. Comparison of calcium (□), phosphorus (○) and iron (◇) counts (edXa) along a line perpendicular to the cuticular layer (site 0) through the superficial enameloid. The sites were approximately 2  $\mu\text{m}$  apart.

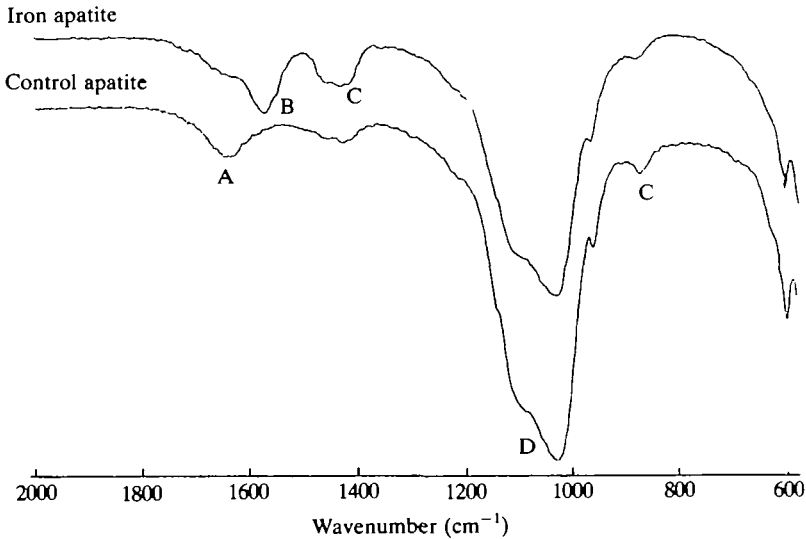


Fig. 14. Infrared spectra of non-doped and iron-doped synthetic hydroxyapatites, A =  $\nu(\text{H}_2\text{O})$ , B =  $\nu(\text{NH}_4^+)$ , C =  $\nu(\text{CO}_3^{2-})$ , D =  $\nu(\text{PO}_4^{3-})$ .

piranha (Shellis and Berkovitz, 1976) it is a mixed inorganic/organic phase. It has been postulated (Preuschoft *et al.* 1974) that the cuticle inhibits the initiation of cracks in the underlying enameloid. Structurally the butterflyfish tooth-cap cuticle would appear to be well suited to this task, being formed from closely packed oriented hydroxyapatite crystals which result in a smooth, fissure-free surface.

There was no morphological or analytical evidence to suggest that discrete iron minerals were present in butterflyfish teeth. Indeed, energy dispersive X-ray

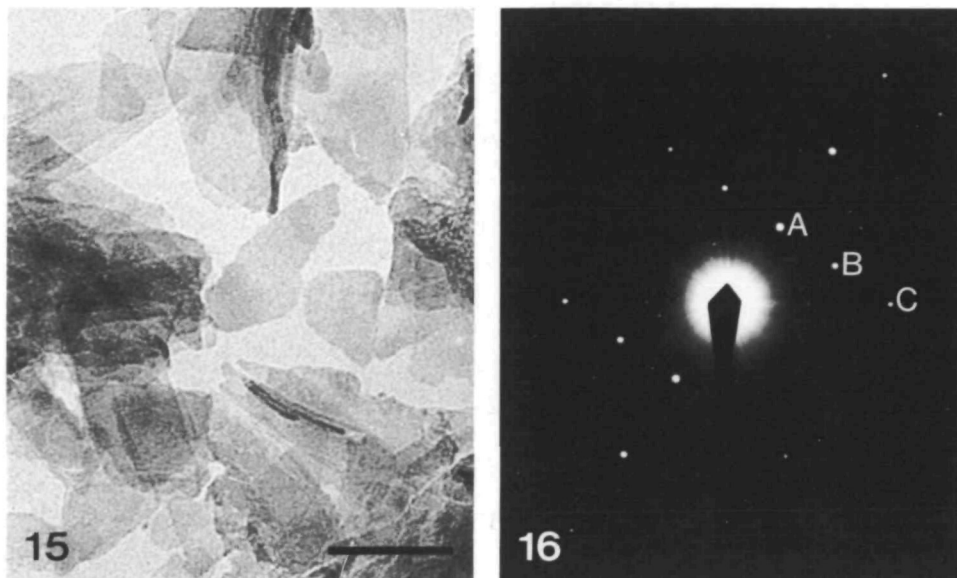


Fig. 15. Image showing plate-like morphology of single crystals of synthetic hydroxyapatite (iron-doped). Scale bar, 100 nm.

Fig. 16. Single crystal electron diffraction pattern of iron-doped synthetic hydroxyapatite. The pattern corresponds to the  $[11\bar{2}0]$  zone of hydroxyapatite, A = (0002), B =  $(1\bar{1}02)$ , C =  $(2\bar{2}02)$ . Camera length 166 cm.

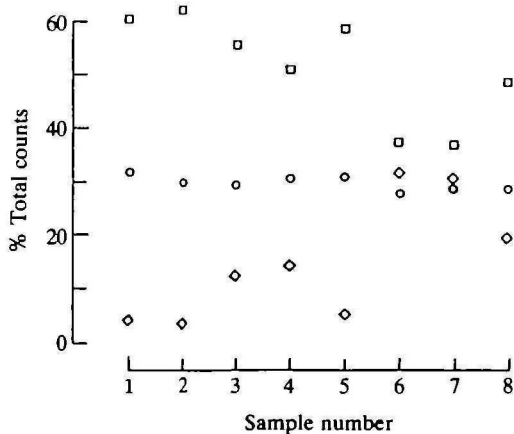


Fig. 17. Comparison of calcium ( $\square$ ), phosphorus ( $\circ$ ) and iron ( $\diamond$ ) counts (edXa) from single crystals of iron-doped synthetic hydroxyapatite.

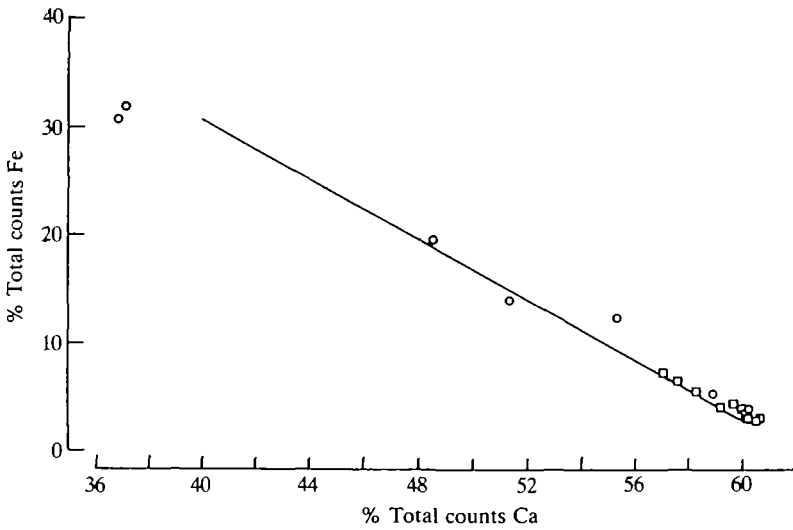


Fig. 18. Linear correlation of iron and calcium counts (edXa) from the cuticular layer (lingual edge) of the tooth cap (□) and the iron-doped synthetic hydroxyapatite (○);  $r = -0.99$ ,  $P < 0.001$ .

analyses showed the levels of iron and calcium within the cuticle to be inversely related to each other, indicating that the iron was closely associated with the hydroxyapatite phase. Similarly, Meridith-Smith (1967) found that the iron-pigmented enamel of urodele amphibians gave electron diffraction patterns consistent with hydroxyapatite, even though the ferritin granules in the adjacent enamel epithelium gave patterns for crystalline  $\text{Fe}_2\text{O}_3 \cdot n\text{H}_2\text{O}$ .

Our results indicate that phosphorus levels were not affected by iron incorporation. Phosphorus levels were the same in the cuticle as in the underlying enameloid. They were also constant among the synthetic iron hydroxyapatite crystals, even though the maximum iron level (30.8%) greatly exceeded iron levels observed in the cuticle (7.5%). These results agree with findings by Okazaki *et al.* (1985) on a series of apatites with increasing iron content. Moreover, phosphorus levels in the cuticle were not significantly different from those in the synthetic crystals.

The stability of the phosphorus levels provides a good internal control for the efficiency of the edXa apparatus. In addition, in both biological and synthetic systems iron and calcium counts were inversely related ( $r = -0.99$ ,  $P < 0.001$ ) and not statistically different, with regression lines of similar ( $P < 0.05$ ) slope and displacement (intercepts). From this we infer that both systems use essentially the same mechanism to incorporate iron into the hydroxyapatite lattice.

Iron occurred in the synthetic hydroxyapatite crystals as  $\text{Fe}^{3+}$  (Mössbauer spectra; D. P. E. Dickson unpublished observations). The linear correlation coefficient between the calcium and iron edXa counts suggests, therefore, that  $\text{Fe}^{3+}$  is substituted into the crystal lattice for a calcium atom, even though it has a

smaller radius (0.064 nm) than calcium (0.099 nm). Since direct substitution results in loss of electroneutrality, it is possible that two calcium ions are replaced for a combination of  $\text{Fe}^{3+}$  and  $\text{NH}_4^+$ . This would explain the presence of the unique N–H vibration in the infrared spectra of the iron-doped sample. This is consistent with the findings of Okazaki *et al.* (1985). The ability of iron and calcium to substitute reversibly for each other within the hydroxyapatite lattice may explain the observation that a marked decrease in the iron pigmentation of rat enamel was associated with a diet high in calcium (Brudevold and Soremark, 1967).

The wide range of iron counts obtained from individual single crystals suggests that iron was distributed heterogeneously throughout the synthetic sample. This was consistent with the broad lines observed in the Mössbauer spectra of this material (D. P. E. Dickson, unpublished data). It is notable that the synthetic hydroxyapatite crystal lattice was able to accommodate iron at levels of about 4% (w/w) without significant lattice distortion. Assuming the same mechanism to be responsible for iron incorporation in both the biogenic and synthetic samples, the cuticular layer is far from being saturated with iron and could have a wide range of iron levels, depending on the iron loading within the system.

The butterflyfish tooth is structurally adapted for feeding from hard surfaces. However, although this study has shown iron to be concentrated at the point of maximal loading, this does not necessarily represent a genetic adaptation leading to increased durability of the cuticle. The small size of the individual tooth caps precluded the use of hardness tests (i.e. diamond indentation) to assess the effect on cuticle strength of increasing iron levels. Motta (1987) assessed iron levels (degree of tooth-cap pigmentation) and reported that species of butterflyfish feeding on the harder coral polyps had raised levels of iron in their teeth. Similarly, Selvig and Halse (1975) reported that the iron-pigmented layer of rat incisor enamel confers increased hardness and increased resistance to 5% formic acid. In contrast, Suga (1984) contended that the incorporation of iron into the cuticular layer of fish teeth was not related to the hardness of the prey or feeding habits. Rather, he suggested that the enameloid provided a storage and detoxification site for excess amounts of iron and fluoride present in the body fluids. This supposition is supported by the fact that teeth are continually being replaced and offer a means of removing these elements into the environment in a stable form.

The incorporation of iron into the synthetic hydroxyapatite lattice decreased the sensitivity of the crystals to damage by the electron beam. The ability of iron to stabilize synthetic hydroxyapatite crystals has also been reported by Okazaki *et al.* (1985). They noted an increase in acid resistance (decrease in crystal solubility) with increasing iron content, which may be of functional importance.

The plate-like morphology of the synthetic iron-doped hydroxyapatite crystals was quite distinct from the biogenic crystals imaged in the cuticular layer. This may be explained by considering the lack of control exerted over crystal growth during the synthesis of the iron-doped synthetic hydroxyapatite, compared with the spatial and chemical control exercised by the biogenic system. The mechanism of iron uptake appears, however, to be common to both systems and, consequently,

we suggest that synthetic iron-doped hydroxyapatite systems are useful models for studying iron incorporation into iron-rich calcified tissues.

### References

- BRUDEVOLD, F. AND SÖREMARK, R. (1967). Chemistry of the mineral phase of enamel. In *Structural and Chemical Organization of Teeth*, vol. 2 (ed. A. E. W. Miles), pp. 247–290. London: Academic Press.
- GARANT, P. R. (1970). Observations on the ultrastructure of the ectodermal components during odontogenesis in *Helostoma temmincki*. *Anat. Rec.* **166**, 167–188.
- HALSE, A. (1973). Effect of dietary iron deficiency on the pigmentation and iron content of rat incisor enamel. *Scand. J. dent. Res.* **81**, 319–334.
- KERR, T. (1960). Development and structure of some actinopterygian and urodele teeth. *Proc. zool. Soc. Lond.* **133**, 401–422.
- LOWENSTAM, H. A. (1967). Lepidocrocite, an apatite mineral, and magnetite in teeth of chitons (Polyplacophora). *Science* **136**, 1373–1375.
- MERIDITH-SMITH, M. (1967). Studies on the structure and development of urodele teeth. PhD thesis, University of London.
- MILES, A. E. W. (1963). Pigmented enamel. *Proc. R. Soc. Med.* **56**, 918–920.
- MOTTA, P. J. (1984). Tooth attachment, replacement, and growth in the butterflyfish, *Chaetodon miliaris* (Chaetodontidae, Perciformes). *Can. J. Zool.* **62**, 183–189.
- MOTTA, P. J. (1985). Functional morphology of the head of Hawaiian and Mid-Pacific butterflyfishes (Chaetodontidae, Perciformes). *Environ. Biol. Fish.* **13**, 253–276.
- MOTTA, P. J. (1987). A quantitative analysis of ferric iron in butterflyfish teeth (Chaetodontidae, Perciformes) and the relationship to feeding ecology. *Can. J. Zool.* **65**, 106–112.
- OKAZAKI, M., TAKAHASHI, J. AND KIMURA, H. (1985). Iron uptake of hydroxyapatite. *J. Osaka Univ. Dent. Sch.* **25**, 17–24.
- PREUSCHOF, H., REIF, W.-E. AND MÜLLER, W. H. (1974). Funktionsanpassungen in Form und Struktur an Haifischzähnen. *Z. Anat. EntwGesch.* **143**, 315–344.
- RANDALL, M. (1966). Electron microscopical demonstration of ferritin in the dental epithelial cells of urodeles. *Nature, Lond.* **210**, 1325–1362.
- REIF, W.-E. (1973). Morphologie und Ultrastruktur des Hai "Schmelzes". *Zoologica Scripta* **2**, 231–250.
- SCHMIDT, W. J. (1958). Zur histologie und Färbung der Zähne des japanischen Riesensalamanders. *Z. Zellforsch. mikrosk. Anat.* **49**, 47–57.
- SCHMIDT, W. J. (1959). Durodentin bei einem Devonischen Fisch (*Laccognathus panderi*). *Z. Zellforsch. mikrosk. Anat.* **49**, 493–514.
- SCHMIDT, W. J. AND KEIL, A. (1971). *Polarizing Microscopy of Dental Tissues* (translated by D. F. G. Poole and A. I. Darling). Oxford: Pergamon Press.
- SELVIG, K. A. AND HALSE, A. (1975). The ultrastructural localization of iron in rat incisor enamel. *Scand. J. dent. Res.* **83**, 88–95.
- SHELLIS, R. P. AND BERKOVITZ, K. B. (1976). Observations on the dental anatomy of piranhas (Characidae) with special reference to tooth structure. *J. Zool., Lond.* **180**, 69–84.
- SUGA, S. (1984). The role of fluoride and iron in mineralization of fish enameloid. In *Tooth Enamel IV* (ed. R. W. Fearnhead and S. Suga), pp. 472–477. Amsterdam: Elsevier Science Publishers BV.